WhiskSight: A Reconfigurable, Vision-Based, Optical Whisker Sensing Array for Simultaneous Contact, Airflow, and Inertia Stimulus Detection

Teresa A Kent, Suhan Kim, Gabriel Kornilowicz, Wenzhen Yuan, *Member, IEEE*, Mitra J. Z. Hartmann, and Sarah Bergbreiter, *Member, IEEE*

***Abstract*—The development of whisker-based sensing systems faces at least two important technical challenges: scaling up the number of whiskers to large arrays while retaining a simple interface; and detecting the wide variety of stimuli that biological whiskers can sense, including both direct touch (contact) and airflow. Here we present the design for a whisker array that leverages a camera to measure whisker rotations without a complex interface. Whiskers are magnetically attached to an elastomer "skin," ensuring that the system is both scalable and reconfigurable. Direct contact is measured from the relative motion between each whisker and the skin, while airflow and inertia can be inferred from the signal experienced by all whiskers in the array. Individual whiskers can resolve the direction of contact transverse to the whisker within 6.2° and whisker rotation magnitude to within 0.5°. An algorithm is developed to distinguish inertial forces from airflow and contact.**

***Index Terms*—Biologically-inspired robots, force and tactile sensing, soft sensors and actuators.**

I. Introduction

WHISKERS, also known as vibrissae, are important tactile sensors for almost all mammals. Mammalian whiskers are arranged in bilateral arrays, with ∼25 or more whiskers emerging from each side of the animal's face [1]. Unlike insect antennae, which have mechanical and chemical sensors along their entire length, mammalian whiskers resemble hairs: sensing occurs only at the whisker base within a densely-innervated follicle [2]. Animals use their whiskers to help with rapid motion planning and navigation, to localize contact with objects, to distinguish object size, shape, texture, and orientation, and to sense fluid flow. Moreover, whisker-based sensing can distinguish between stimuli that occur simultaneously (e.g., contact can be distinguished from the inertial forces generated by the animal's own motion).

Not surprisingly, engineers have tried to replicate these sensory systems on robots for similar tasks. Several engineered systems have exploited whisker bending to perform contact point determination with a single whisker [3]–[7]. Other studies have used whiskers primarily as contact/non-contact detectors to develop algorithms that orient the entire array towards an object [8]–[10]. Yet other whisker-inspired sensors have been designed to detect non-contact mechanical stimuli such as flow (e.g., [4], [11]–[13]). Ultimately – if the full capabilities of the biological system are to be realized in hardware – these approaches will need to merge, but important technical challenges remain.

The first challenge involves the number of whiskers in an engineered array, especially if detailed information about individual whisker bending is to be retained. Natural whiskers each have their own complex, multi-dimensional transduction mechanism [2]. In an engineered system, adding transducers to each whisker significantly increases computational and hardware complexity. The largest engineered whisker arrays have used 18 [10] and 20 [9] whiskers with one transducer per whisker. By capturing deflections and (motor-controlled) rotations of each whisker, these arrays could determine the identities of the whiskers that made contact and then orient the array to a detected object. Although these arrays are impressive engineering feats, they are costly and complex; wiring scales with whisker number.

An alternative approach, taken by "TacWhiskers," uses a single camera as the transducer for a whisker array [14], similar to the approach used by several recent non-whisker tactile sensors (e.g., [15]–[17]). Although modern cameras use millions of photoreceptor-like elements, we classify a camera as a single transducer in this work because it has a single interface. The TacWhiskers used a modified version of the TacTip sensor described in [15]; a camera monitors the movement of 3D printed pillars beneath a domed array of whiskers. The whiskers were reported highly accurate during convergent whisking contact of an array of ten whiskers.

Manuscript received October 15, 2020; accepted February 11, 2021. Date of publication March 1, 2021; date of current version March 23, 2021. This letter was recommended for publication by Associate Editor M. Gauthier and Editor D. Popa upon evaluation of the reviewers' comments. This work was supported by NSF Grant BCS-1921251. This work began as a project for the Tactile Sensing and Haptics course in the Robotics Institute at Carnegie Mellon. *(Corresponding author: Teresa A Kent.)*

Teresa A Kent and Wenzhen Yuan are with Robotics Institute, Carnegie Mellon University, Pittsburgh, PA 15213 USA (e-mail: tkent@andrew.cmu.edu; yuanwz@cmu.edu).

Suhan Kim, Gabriel Kornilowicz, and Sarah Bergbreiter are with Mechanical Engineering Department, Carnegie Mellon University, Pittsburgh, PA 15217 USA (e-mail: suhank@andrew.cmu.edu; gkornilo@andrew.cmu.edu; sbergbre@andrew.cmu.edu).

Mitra J. Z. Hartmann is with Biomedical Engineering and Mechanical Engineering Departments, Northwestern University, Evanston, IL 60208 USA (e-mail: hartmann@northwestern.edu).

This letter has supplementary downloadable material available at https://doi.org/10.1109/LRA.2021.3062816, provided by the authors.

Digital Object Identifier 10.1109/LRA.2021.3062816

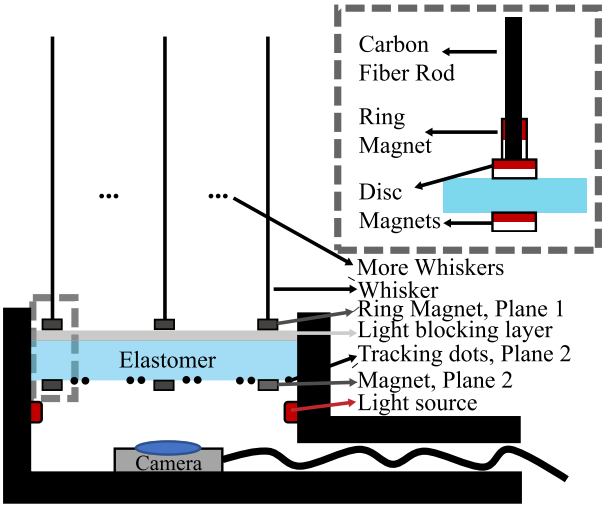

Fig. 1. A schematic of the WhiskSight sensor. Whiskers (rigid carbon fiber rods) are attached to an elastomer membrane suspended above a camera. The attachment is magnetic, using a disc magnet attached to the whisker on top of the membrane and another disc magnet below the membrane. The camera captures whisker rotations along with the motion of tracking dots on the membrane. A light blocking layer and internal LEDs ensure consistent lighting. The image is not to scale.

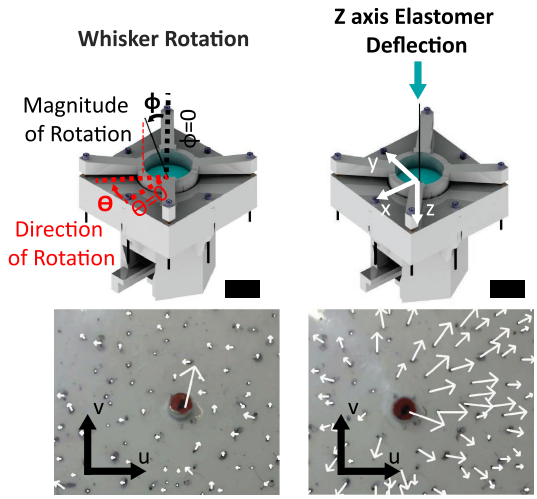

Fig. 2. Coordinate systems for stimuli applied to rigid whiskers. Top row: The angles θ and ϕ (degrees) represent the direction and magnitude of whisker rotation from nominal (perpendicular to the elastomer membrane). The 'z-axis deflection' quantifies displacement in millimeters as the whisker moves parallel to its z-axis. Scale bars = 30 mm. Bottom row: The images show typical camera output for whisker rotation (left) and z-axis deflection of the elastomer (right). The motion of a tracker dot on the whisker magnet or the elastomer is described as 'translation' in a u-v coordinate system. In both images, arrow magnitudes show translation of the dots scaled by 10x for visual clarity. Scale: magnet diameter (red circle) is 3.2 mm.

A second challenge is that a wide variety of stimuli – with amplitudes that can vary over several orders of magnitude – can impart forces and motions to the whiskers. Direct contact (touch), airflow, and motion at the whisker base (which we will call inertial) stimuli can all be sensed by whiskers. Discriminating between these various stimuli is still an unmet challenge. We are aware of only two papers that demonstrated a single whisker that could detect (but not distinguish between) contact and flow [12], [18]. This is a notable gap, as airflow, inertia, and contact are all realistic stimuli that could be introduced as intentional or confounding variables in robotic implementation [19].

The primary contribution of this paper is to show that a reconfigurable, vision-based whisker array sensor (WhiskSight) can sense and discriminate between multiple stimuli. Building on the TacWhiskers approach ([14], [15]), the present work uses a variation on the GelSight tactile sensor [16] to measure whisker rotations and to distinguish between contact, airflow, and inertial stimuli (Fig. 1). Whiskers are magnetically attached to a light-blocking elastomer membrane suspended above a camera. Magnetic attachments ensure modularity, scalability, and reconfigurability. Using a commercially available USB camera we demonstrate that the system can simultaneously gather information about whisker rotations in a 6-whisker array. Similar to the GelSight tactile force sensor [16], FingerVision [20], and GelForce [21], we use markers on the elastomer membrane to track deformations of the membrane in addition to the whisker movements. This extra information allows us to discriminate between different stimuli (contact, airflow, inertial) as well as to detect the direction and magnitude of individual whisker rotations regardless of rotations and deflections elsewhere in the array. Notably, WhiskSight achieves these capabilities even though it is not actuated. This new approach to whisker sensing could enable robotic navigation and obstacle detection/avoidance in low visibility settings without confounding data from system motion or airflow.

II. WhiskSight System Design

The WhiskSight system design is based on a scaled up version of the GelSight sensor [16] and is illustrated in Fig. 1. The system includes a camera, an elastomer membrane, magnetically attached rigid whiskers, and a light source. The elastomer membrane, held in tension, suspends the whiskers over the camera. The camera senses rotations and deflections of each whisker. As seen in Fig. 2, θ represents the whisker 'rotation direction,' ϕ represents the 'rotation magnitude,' and 'z-axis deflection' represents a deflection of the elastomer membrane parallel to the whisker z-axis, typically caused by an axial force applied to a whisker.

More specifically, the camera tracks translation of the magnets as well as the tracking dots painted on the bottom surface of the elastomer membrane in the image plane described by u-v coordinates (Fig. 2). Software correlates these translations back to rotations applied to individual whiskers. The light source internal to the sensing system decreases the effect of ambient lighting on the camera image, thereby improving consistency of the tracking algorithm.

A. Mechanical System

To enable reconfigurability, whiskers are attached with magnets to the elastomer membrane as shown in Fig. 1. Each whisker consists of a 1 mm diameter, 100 mm long carbon fiber rod glued into a ring magnet, which is then glued on a disc magnet. Unlike

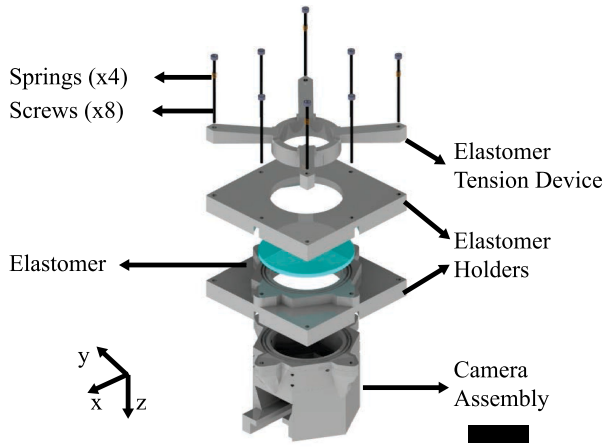

Fig. 3. Assembly of the physical system. Scale bar represents 50 mm.

biological whiskers, which are flexible and have taper, the carbon rod whiskers are stiff and have constant diameter. Using magnets on both the top and bottom of the membrane, whiskers can be attached anywhere within camera view. The disc magnets are 3.175 mm diameter, 1.58 mm thick nickle-plated NdFeB axial force magnets (DH11, KJ Magnetics). The ring magnets are 3.175 mm outer diameter, 1.58 mm thick nickle-plated NdFeB axial force magnets (R211, KJ Magnetics) with a pull force of 0.31 pounds.

The rest of the sensing system is modular. The camera (Logitech HD Webcam C310) can be slotted into a hexagonal 3D printed camera assembly. This assembly holds the LEDs (LilyPad, DEV-13 902) used as a light source halfway up the casing with wire pass-throughs in the casing (Fig. 3). The elastomer membrane is ≈ 1 mm thick PDMS (Sylgard 184, Dow Chemical). The top of the PDMS is painted white with acrylic paint and black dots are made with marker on the bottom. The top and bottom holders clamp the elastomer in place, after which a tensioner is used to push the elastomer membrane downward to place it in tension. The tension in the elastomer can be adjusted by tightening the tensioner screws. The whiskers are added to the system only after the elastomer is in tension so that magnetic interaction does not affect the elastomer tension (Supplementary Video). Finally, the entire system is placed over the camera assembly and screwed into place. It should be noted that this setup is designed to test and characterize the whiskers; a robotic implementation could be made far more compact.

B. Whisker and Membrane Tracking

Typical views captured by the camera can be seen in Fig. 2. The entire bottom of the magnet is painted red/orange so that the whiskers' locations can be more easily resolved and to reduce light reflection from the magnets. Black tracker dots are marked on both the bottom of the elastomer and the bottom of the magnets using a permanent marker. The dots and whiskers are initially identified using a custom segmentation algorithm, then tracked during tests using various tracking algorithms; Minimum Output Sum of Squared Error Tracker (MOSSE) [22] was chosen for its accuracy and speed, and Channel and Spatial Reliability Tracker (CSRT) [23] was chosen for its accuracy. Validation tests demonstrated that MOSSE could track over 50 dots at 17 frames per second. Depending on the task, the tracker was either applied to pre-recorded videos, previously captured and labeled sequential images, or to live video.

Whisker rotation can be calculated using the translation of the whisker magnet in the image plane, δu and δv.

$$\theta = \arctan\left(\delta u / \delta v\right) \tag{1}$$

Calculating rotation magnitude requires knowledge of camera and geometric parameters including u and v axis resolution (u_{res} and v_{res}), u and v angle of view (u_{aov} and v_{aov}), distance between the camera and membrane (ΔZ), and the height of the magnet (h_{mag}) [24]. These parameters are used to calculate the average mm per pixel (ρ); because the camera's resolution (pixels/mm) is not identical in the u and v directions, we average the two.

ϕ can then be calculated with these parameters assuming that the points of interest all occur in a plane ΔZ away from the camera parallel to the image plane. Eqn. 3 converts the translation of the bottom of the magnet (pixels) into millimeters and then uses the known height of the magnet to obtain the rotation magnitude, assuming the translation is primarily in-plane.

$$\rho = \frac{1}{2}\left(\frac{\Delta Z}{u_{res}}\tan\left(u_{aov}\right) + \frac{\Delta Z}{v_{res}}\tan\left(v_{aov}\right)\right) \tag{2}$$

$$\phi = \arctan\left(\rho\sqrt{\delta u^2 + \delta v^2}/h_{mag}\right) \tag{3}$$

In the whisker system shown in Fig. 3, $h_{mag} = 1.58$ mm and $\Delta Z = 54$ mm. For the chosen camera, $u_{res} = 1280$ pixels, $v_{res} = 720$ pixels, the angle of view in the u-direction $u_{aov} = 26.95^\circ$, and v-direction $v_{aov} = 16.26^\circ$. The z-axis deflection was not calculated but was accounted for using the movement of the dots surrounding each whisker. This motion was previously characterized in [16].

To determine whisker motion independent of membrane motion (which could be affected by neighboring whiskers or other stimuli), the membrane tracking dots closest to the whisker magnet were found using the L2 norm for distance. The average translation along u and v (pixels) of the k nearest dots was subtracted from the translation (pixels) of the whisker magnet. We ensured that dots were spaced at regular angular intervals around the whisker magnets.

III. Contact Characterization

To start, the whisker rotations and deflections that occur from direct touch (contact) with a whisker are characterized.

A. Experimental Setup

A Thorlabs manual stage with two linear axes and one rotation axis was used to apply known rotation directions (θ) and magnitudes (ϕ) to a single whisker (Fig. 4a). To test the system's response to various whisker rotation directions, θ was incremented from 0° to 360° in 10° steps while ϕ was fixed at 7°. Whisker rotation magnitude, ϕ, was characterized by rotating

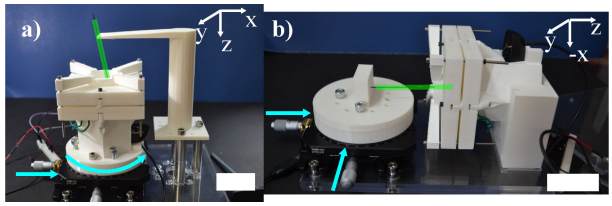

Fig. 4. a) A test setup in which rotation magnitude (ϕ) and direction (θ) can be controlled. b) A test setup that can apply z-axis deflections and rotation about the y-axis. Scale bars = 50 mm. In both figures a green line has been drawn over the whisker for visual clarity. Cyan directional arrows indicate directions of stage motion.

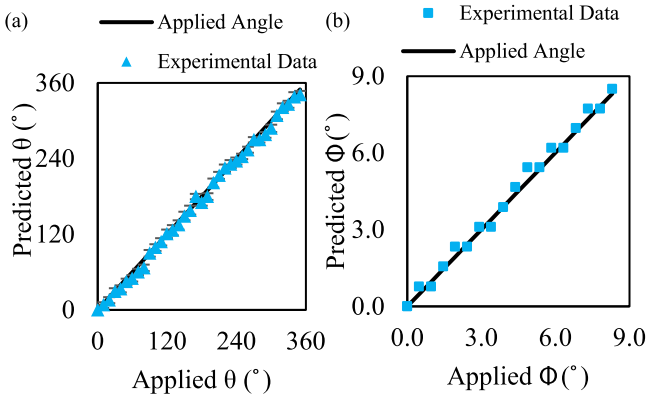

Fig. 5. a) The value of θ predicted from the camera image (blue triangles) is compared to the value of θ applied by the testing system (black line). Error bars represent the full range of possible values for θ that a given u, v pixel location could represent. b) The value of ϕ predicted from the camera image (blue squares) versus applied ϕ (black line).

the whisker in 0.49° increments along the positive x-axis. Linear translations of the stage used to deflect the whisker are converted to angles using the known geometry, and the MOSSE tracker was used to track dots.

Next, using the setup shown in Fig. 4b, we evaluated how rotation measurements would be affected by z-axis deflections. We hypothesized that z-axis deflections could be subtracted from the total motion by monitoring both the magnet translation and the nearby elastomer membrane translation. The whisker was rotated about the x-axis ($\theta = 90^\circ$) from -2.77° to 2.77° in 21 equal steps. Each test was repeated with z-axis deflection ranging from 0 mm to 5 mm. Because this experiment used very small angular increments (0.29°), the tracker was changed to OpenCV's CSRT tracker, which has better (sub-pixel) accuracy than MOSSE.

In a separate set of experiments, we tested the effect of z-axis deflections when the whisker was placed at two different offsets (small and large) from the image center. The offsets determine how the whisker magnet will translate in the camera image during a pure z-axis deflection. If the magnet is centered in the camera image, it will appear to grow in size while staying fixed in position. If the magnet is offset from the image center, it will not only appear to grow in size but also appear to translate in the camera image. If the offset is too large, the magnet will ultimately translate out of the image for a sufficiently large z-deflection [24].

The final characterization of contact stimuli tested a whisker array. Contact on other whiskers in the array or other stimuli like airflow applied to the whiskers can make it challenging to detect contact on an individual whisker. In the WhiskSight sensor, the relative motion between the elastomer membrane and whisker magnets can be used to determine contact. If the difference between the net translation of the elastomer dots surrounding a whisker and the translation of the whisker magnet was greater than a threshold, contact was indicated. To test this approach, we applied rotations to single whiskers in a 6-whisker array, and recorded if the correct whisker was indicated as the one in contact. In addition, we monitored all of the other whiskers to evaluate if they falsely reported contact or correctly reported no contact (false positives and true negatives). We then applied a z-axis deflection to one of the whiskers in the array and repeated the contact test on the remaining five whiskers, recording all true positives, false positives, and negatives. Each of these experiments was repeated twice. Two metrics were used to evaluate the accuracy of different threshold values: the percentage of true positives and percentage of true negatives.

B. Experimental Results

Whiskers were first characterized with contact applied to individual whiskers. Fig. 5a shows a high-quality fit (RMS error $= 6.2^\circ$) between the applied rotation direction, θ, and the whisker rotation predicted from the camera image. The error is slightly larger than the theoretically best achievable accuracy of our system (5.35°) due to discrete pixel displacements. With a higher resolution camera, we would expect the accuracy to increase. In addition, as rotation magnitude, ϕ, increases, the direction accuracy is expected to improve due to larger δu and δv in Eqn. 1.

Limitations imposed by camera resolution are easily observed in Fig. 5 b, which plots measured rotation magnitude, ϕ, versus the experimentally-applied rotation magnitude. At each step a 0.49° increase in ϕ was applied, but the dot on the whisker magnet does not always translate to a new pixel with each step. Based on camera and geometric parameters, an accuracy of 0.5° is expected for ϕ. The measured mean RMS error between the applied ϕ and the predicted ϕ angle is 0.25° – close to the expected accuracy. The accuracy of ϕ is significantly higher than the accuracy of θ. This result can be explained by two factors. First, 1° of rotation in ϕ causes significantly more pixel movement than 1° in θ. Second, the experimental measurement of ϕ was limited to motion along a single axis.

The rotation testing described above was performed without z-axis deflections. Membrane deflection is of particular concern because it changes the distance between the camera and elastomer surface, which is assumed constant in Eqn. 3. The nominal distance between the camera and membrane is small (54 mm), increasing the possible effect of small deflections. Translation during elastomer deflection can be further magnified when the whiskers are offset from the camera center, and this offset varies significantly across a whisker array. In Fig. 6, it is clear that measured translation due to applied z-axis deflection differs

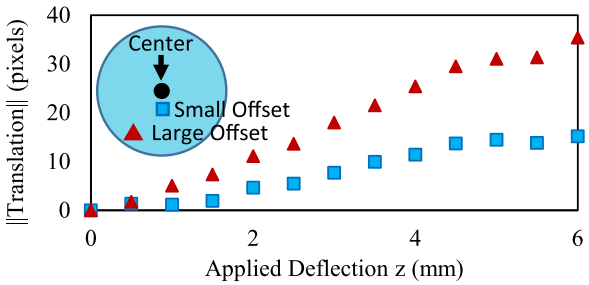

Fig. 6. As the whisker location moves away from the center of the camera image, z-axis deflection has an increasingly large effect on the magnet's apparent translation in the camera image. This is represented as L2 norm of $(\delta u, \delta v)$. A whisker at the camera center would have zero translation.

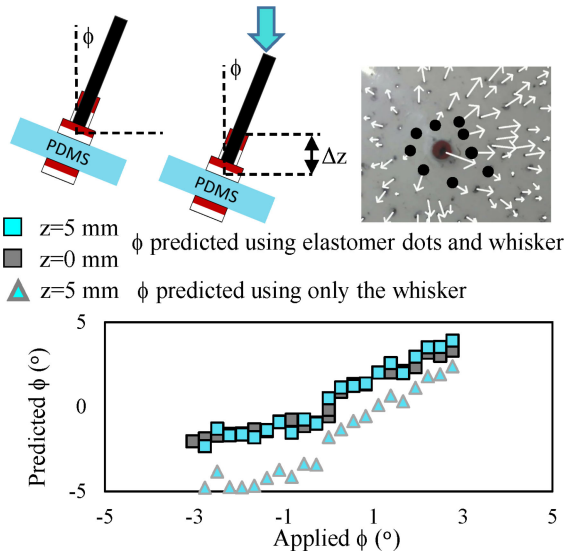

Fig. 7. By subtracting the average translation of the nine closest elastomer dots (white arrows, 10x magnification) from translation of the dot on the magnet (red base), we can more accurately predict the angle ϕ during whisker deflection. The predicted ϕ that uses only the whisker translation (blue triangles) is significantly offset from the "zero curve" (grey squares). ϕ predicted using this subtraction method (blue squares) removes this offset, resulting in accurate predictions even under z-axis deflection.

greatly depending on the whisker offset in the camera image; a deflection applied to a whisker at large offset is (incorrectly) predicted as three times the magnitude of the same deflection applied to a whisker with a small offset. Without mitigation this could have a detrimental affect to measuring independent whisker rotations in an array.

Fortunately, by tracking the membrane dots in addition to whisker magnets we are able to overcome this possible problem. As illustrated in Fig. 2, during whisker rotation the pixel translation is mostly limited to the bottom of the magnet but in z-axis deflection the entire membrane moves. Using the experimental setup seen in Fig. 4b we were able to test our ability to remove the effect of z-axis deflection. We subtracted the average translation of the nine elastomer dots closest to a whisker undergoing a rotation about the x-axis while the membrane was deflected from 0 mm to 5 mm in 0.5 mm increments.

We first defined the "zero curve" as the ϕ predicted using this subtraction method when zero deflection was applied. Results shown in Fig. 7 revealed that the 5 mm prediction curve shifts to align with the zero deflection curve when elastomer translation is taken into account. With this subtraction method, the RMS error between the zero curve and other curves was an average of $0.37°$, whereas without the subtraction method the RMS error grew aggressively up to $1.79°$ at 5 mm deflection. Only the 0 mm and 5 mm deflection results are shown in Fig. 7 for clarity.

Exploiting the ability to isolate rotations from z-axis deflections, we tested an algorithm to distinguish tactile contact applied to individual whiskers in an array. When one whisker in an array is rotated or deflected, the resulting translation of the elastomer membrane could show up as unintended noise for other whiskers in the array. To account for this, contact for each whisker of a six-whisker array was indicated by a significant difference between the translation of the whisker magnet and the net translation of the closest six membrane dots to the whisker magnet. Six dots were chosen instead of nine to reduce any influence from nearby whiskers in the array. The translation threshold for significance was an independent variable. A key tradeoff in this approach is the minimum rotation magnitude, ϕ, required to indicate contact. Lower thresholds are more likely to pick up noise from surrounding whiskers while a large threshold requires a much larger whisker rotation to achieve the necessary pixel translation.

The first two trials rotated a single whisker only. In the second two trials, one whisker was deflected along the z-axis to deform the membrane while other whiskers were rotated. When the threshold was small (0 or 1 pixel) the accuracy of detection was reduced to 80% because of the large number of false positives. Using a higher threshold of 4 or 5 pixels resulted in only one false negative during the deflection plus rotation trials. In these large threshold cases, the required rotation magnitude is also expected to be relatively large ($\approx 6°$ to $8°$). As a result, a contact threshold of 3 pixels was chosen as the best threshold for future tests given the balance of high accuracy and small ϕ required to trigger the contact condition (Supplementary Video).

IV. Airflow and Inertial Stimuli Characterization

After quantifying the response of whiskers to contact stimuli, we sought to understand the response to airflow and whisker motion due to inertial effects.

A. Experimental Setup

To study the effects of airflow, the whiskers were subjected to high, medium and low flow speeds using a 10 A Stanley fan (Model 655 704). No attempt was made to make the flow laminar, as we were primarily interested in detection of airflow that may naturally occur in an environment. Airflow velocity was not measured. In a second airflow experiment, contact was applied to an individual whisker simultaneously with the airflow stimuli (Supplementary Video).

Active whisking in rodents is known to generate inertial effects [25], [26]. To approximate actuated, inertial whisking, the full whisker system (Fig. 3) was rotated back and forth manually

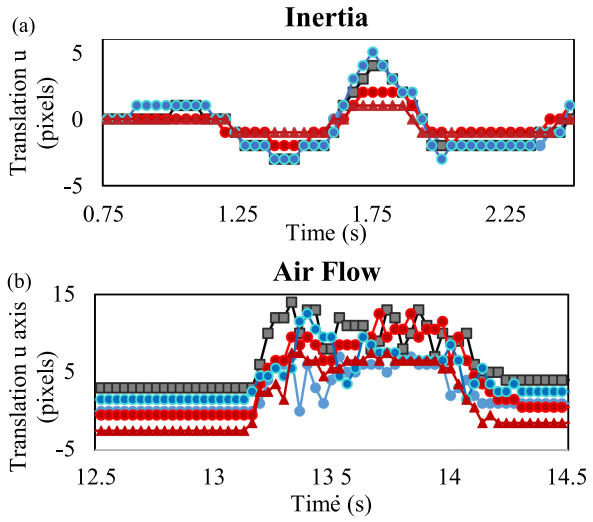

Fig. 8. Response to a) inertial stimuli, and b) airflow stimuli. Both plots show the measured response of five of the six whiskers in the array. The same whiskers are shown in each panel and the colors are matched by whisker.

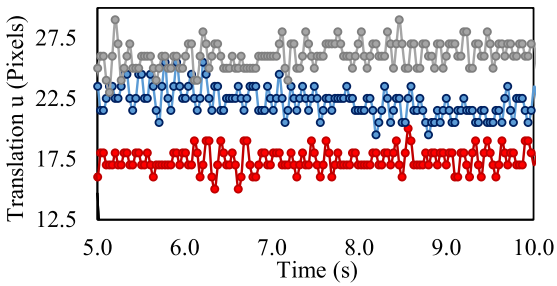

Fig. 9. The response of one whisker in the array to airflow of low (red), medium (blue) and high (gray) speeds in steady state. Although responses to the three speeds have different mean values, the oscillation frequency is similar for all speeds.

(Supplementary Video). Active whisking can confuse robotic systems [19] but poses no problems for animals. Rotations and translations were performed around both the x and y axes to better understand the signals generated under base excitations.

B. Experimental Results

When the whiskers undergo rotations due to airflow and inertial stimuli, the signals differ significantly, especially in frequency (Fig. 8). In addition, a key distinction from the contact stimuli discussed previously is that these non-contact mechanical stimuli generally affect all whiskers in an array similarly.

Consistent with results from rodent whiskers [27], the varying flow speeds are primarily characterized by changes in the mean rotation magnitude as seen in Fig. 9. This figure describes translation of one whisker in the array once its response has reached steady state. Translation of each whisker in the array as well as transients can be seen in Fig. 8b. A whisker's response to airflow has two characteristic features: the translation oscillates, and the average whisker translation is significantly ($\approx 5\times$) larger than the translation of the elastomer membrane (Supplementary Video). Although the mean translation depends on flow speed,

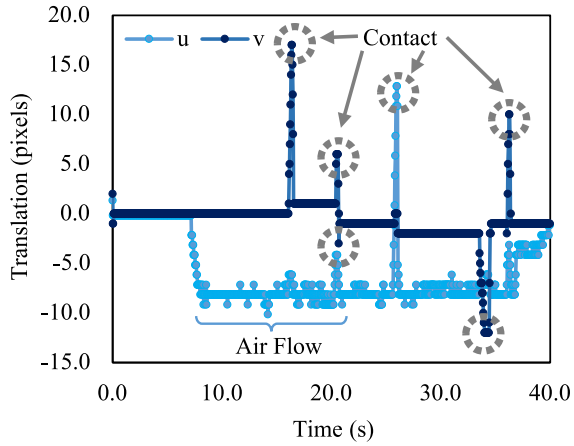

Fig. 10. Translation in u and v of a single whisker in response to simultaneous contact and airflow. The characteristic oscillation is visible in the u translation parallel to the flow, while contact is observable in both u and v depending on the whisker rotation direction. (Supplementary video).

the oscillation patterns are consistent across the flow magnitudes. This frequency of the oscillation pattern can be explained by the flow turbulence, the whisker's intrinsic dynamics, and the natural compliance and damping properties of the elastomer.

We also demonstrated that the system could sense contact in the presence of airflow (Supplementary Video). In Fig. 10, medium speed airflow is applied across an array of whiskers in the +x direction (a single whisker is plotted for clarity). Contact events are observed as clear data spikes relative to the consistent translation from airflow. The contact is applied with varying rotation directions, θ, as evidenced by spikes with varying u and v magnitudes. It is important to note that contact in airflow will be more challenging to distinguish if a contact stimulus is applied to many whiskers.

Fig. 8a shows the translation of the whiskers when a large acceleration was applied to the whisker sensing system (Supplementary Video). Like airflow, inertial forces generated by motion of the base cause all whiskers to move in a very similar pattern. However, the response to an inertial translation can be distinguished from airflow by the frequency content: inertial motion results in relatively smooth, low frequency whisker translation when compared to the higher frequency oscillations associated with airflow.

In addition, the elastomer membrane translation is much more significant during an inertial stimulus in comparison to airflow (Supplementary Video). Fig. 11 plots the translation of a whisker and its six closest membrane dots in response to a base excitation. The figure shows that the six dots' responses to base excitation are remarkably similar to the response of the whisker. In other words, the whiskers and the elastomer membrane translate similarly in response to inertial stimuli. This is a key feature that will be used to distinguish contact from base excitation. However, it should be noted that a relatively large acceleration is required to capture inertial motion.

The differences in characteristics between airflow and inertial stimuli conforms with what we know about the physical sensing system. The airflow tests did not interact with the elastomer which was shielded by the protective casing but the whiskers

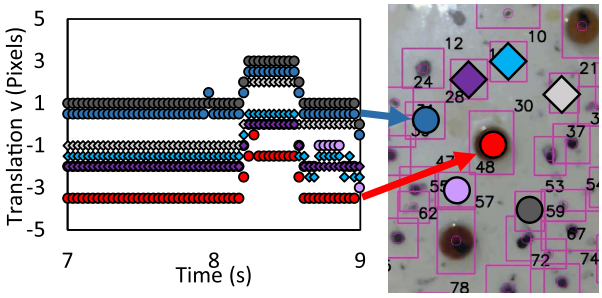

Fig. 11. The translations of a whisker and its six closest elastomer dots are shown while the base of the system is accelerated along the system's y-axis. (Supplementary video).

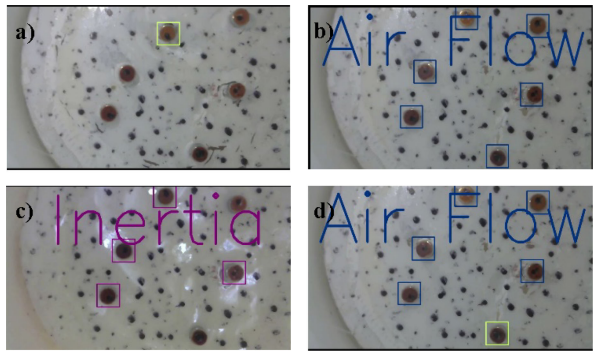

Fig. 12. Frames from the supplementary video show that the WhiskSight can correctly classify varying applied stimuli: a) a single whisker in contact (green), b) the entire system exposed to medium speed airflow (blue), c) the WhiskSight base accelerated to generate inertial stimuli (purple), and d) the system exposed to medium speed airflow with a whisker in contact.

experienced drag forces. Turbulent flow resulted in oscillatory behavior of the whiskers but no displacement of the membrane. In contrast, inertial forces affect the entire system as seen by motion in both the elastomer membrane and whiskers. The inertial forces reflect accelerations of the sensing system while constant velocity would be identified as airflow if that velocity is large enough.

V. Classifying Stimuli

To distinguish between touch contact, airflow, and inertial stimuli, a new algorithm was developed and tuned based on results from the contact, airflow, and inertial characterization experiments. Eqn. 4 converts whisker directional translations in image coordinates, δu_i and δv_i, into the magnitude of whisker movement, $\delta W_{mag,i}$. In the equation below, i is used to index each whisker.

$$\delta W_{mag,i} = (\delta u_i^2 + \delta v_i^2)^{1/2} \tag{4}$$

The stimuli on each whisker is classified by 1) checking if the whisker has moved ($\delta W_{mag,i} >= 3$), and 2) determining the types of stimulus. For an inertial stimulus, the whisker magnet and membrane dots move together (Fig. 11), while only the whisker dots move for airflow stimuli. Airflow is also indicated by higher frequency oscillations around a central offset magnitude (Fig. 9, 10) which are tracked by counting the number of direction changes within the previous 20 frames (corresponding to 0.66 s). If over half the full number of whiskers detect airflow or inertial stimuli (which should affect all similarly), the system is classified as detecting the relevant stimulus. If fewer than half of the whiskers have moved, contact is indicated. Contact can be detected simultaneously with airflow or inertia by then checking to see if any whisker's translation vector deviates significantly from the average. Further detail, including specific thresholds, can be found in the source code uploaded to our GitHub repository [28]. This approach works well for a small system of six whiskers, but would likely need to be modified for larger arrays in which large groups of whiskers may be in contact.

This algorithm was used on a new video in which all stimuli were present, sometimes simultaneously (contact, airflow, inertia, and airflow with contact). For these tests we used the CSRT tracker as inertia required a higher tracking accuracy. The array was able to identify stimuli correctly each time and individual whiskers were accurate most of the time (Supplementary Video, Fig. 12). The individual whisker errors are most likely the result of tracker drift and could continue to be improved for future robotic implementations.

VI. Discussion and Future Work

Here we demonstrated how a whisker variant of the GelSight sensor can help create larger whisker arrays and allow us to distinguish between various stimuli (contact, airflow, and inertial) by tracking the motion of both the flat, elastomer membrane, along with motion of the individual whiskers. A single camera was used to track an array of six whiskers along with the elastomer membrane, significantly decreasing the complexity and interface required for a whisker array. In addition, the WhiskSight used magnetic attachment for reconfiguration of the array as needed for specific applications. While our demonstrations were made using an array of six whiskers, the magnetic attachment makes it relatively straightforward to scale up to larger arrays. The magnetic attachment also presents a limitation on array spacing however; the minimum spacing between whiskers is determined by forces between the magnets. As the magnetic force increases, the attachment force to the elastomer membrane increases but the minimum distance between whiskers also increases due to interactions between the magnets. This work favors attachment force over larger arrays, but future work can determine more optimal magnet sizing. In addition, if reconfigurability is not required, adhesives and other non-magnetic whisker attachments (e.g., [14]) could be used. Magnetic attachment also influences the choice of marker locations on the elastomer membrane; the benefits of markers in a regular grid pattern, random marker locations (as in digital image correlation, DIC), or markers spaced regularly around magnet locations are ideas to explore in future work.

Another key feature in the whisker array presented in this work was the use of a flat elastomer membrane. The ability to classify contact, airflow, and inertial stimuli emerges from our ability to track both the motion of individual whiskers and

the motion of the elastomer membrane oriented parallel to the camera image plane. Domed and curved surfaces found in other sensors like the TacTip [15] and TacWhiskers [14] provide greater surface area visible by the camera. The parallel planes trade off surface area for consistent motion across the array. For example, constant airflow across the array along with similar whisker sizes will result in similar drag profiles and therefore similar motions in the image plane of the camera. In general, an elastomer membrane parallel to the image plane simplifies the math between motion of the elastomer membrane and motion in the camera image. Finally, because the elastomer membrane is not exposed to airflow, the whisker array can respond to airflow and inertial stimuli differently, simplifying classification of these two stimuli.

Finally, the presented whisker sensing system still has several avenues for improvement in future work. In this work, whiskers were characterized for accuracy in 3 DOF (ϕ, θ, and z-axis deflection), and conform to the expected performance of the system given the choice of camera and geometry. These degrees of freedom were assumed to be most important to determine whisker motion, but future iterations of the whisker system could validate this by tracking additional degrees of freedom by increasing the number of tracked markers on the whisker magnets (e.g., corners of square or rectangular magnets). In addition, current system performance is largely limited by choice of camera. Higher pixel counts per unit area could improve the rotation and z-axis deflection resolutions. Higher frame rates could speed up the time to detect various stimuli. The whiskers themselves can also be modified; identical rigid whiskers were used in this implementation, but flexible and tapered whiskers could ultimately help identify contact location along each whisker [6]. Finally, adding actuation through pneumatics or some other method can provide additional information about contacts, especially given the ease of distinguishing contact from the motion of the whisking system. Overall, the ability to detect and classify various stimuli like airflow, inertia and touch opens possibilities for future robotic applications of the system as well as for physical models of various biological whisking systems.

ACKNOWLEDGMENT

The authors would like to thank the course TA, Arpit Agarwal, for assistance.

REFERENCES

[1] M. N. Muchlinski, J. R. Wible, I. Corfe, M. Sullivan, and R. A. Grant, "Good vibrations: The evolution of whisking in small mammals," *Anat. Rec.*, vol. 303, no. 1, pp. 89–99, 2020.

[2] S. Ebara, K. Kumamoto, T. Matsuura, J. E. Mazurkiewicz, and F. L. Rice, "Similarities and differences in the innervation of mystacial vibrissal follicle-sinus complexes in the rat and cat: A confocal microscopic study," *J. Comp. Neurol.*, vol. 449, no. 2, pp. 103–119, 2002.

[3] M. Kaneko, N. Kanayama, and T. Tsuji, "Active antenna for contact sensing," *IEEE Trans. Robot. Automat.*, vol. 14, no. 2, pp. 278–291, Apr. 1998.

[4] J. H. Solomon and M. J. Hartmann, "Robotic whiskers used to sense features," *Nature*, vol. 443, no. 7111, pp. 525–525, 2006.

[5] J. H. Solomon and M. J. Hartmann, "Extracting object contours with the sweep of a robotic whisker using torque information," *Int. J. Robot. Res.*, vol. 29, no. 9, pp. 1233–1245, 2010.

[6] H. M. Emnett, M. M. Graff, and M. J. Hartmann, "A novel whisker sensor used for 3D contact point determination and contour extraction," in *Robot.: Sci. Syst.*, vol. XIV, 2018.

[7] M. H. Evans, C. W. Fox, N. F. Lepora, M. J. Pearson, J. C. Sullivan, and T. J. Prescott, "The effect of whisker movement on radial distance estimation: A case study in comparative robotics," *Front. Neurorobot.*, vol. 6, 2013, Art. no. 12.

[8] T. J. Prescott, M. E. Diamond, and A. M. Wing, "Active touch sensing," *Philos. Trans. R. Soc. Lond. B. Biol. Sci.*, vol. 12, no. 366, pp. 2989–2995, Nov. 2011.

[9] T. Assaf, E. D. Wilson, S. Anderson, P. Dean, J. Porrill, and M. J. Pearson, "Visual-tactile sensory map calibration of a biomimetic whiskered robot," in *Proc. IEEE Int. Conf. Robot. Automat.*, 2016, pp. 967–972.

[10] M. J. Pearson, B. Mitchinson, J. C. Sullivan, A. G. Pipe, and T. J. Prescott, "Biomimetic vibrissal sensing for robots," *Philos. Trans. Roy. Soc. B: Biol. Sci.*, vol. 366, no. 1581, pp. 3085–3096, 2011.

[11] S. Kim, R. Kubicek, A. Paris, A. Tagliabue, J. P. How, and S. Bergbreiter, "A whisker-inspired fin sensor for multi-directional airflow sensing," in *Proc. IEEE/RSJ Int. Conf. Intell. Robots Syst.*, 2020, pp. 1330–1337.

[12] W. Deer and P. E. Pounds, "Lightweight whiskers for contact, pre-contact, and fluid velocity sensing," *Proc. IEEE Robot. Automat. Lett.*, vol. 4, no. 2, pp. 1978–1984, Apr. 2019.

[13] K. Takei, Z. Yu, M. Zheng, H. Ota, T. Takahashi, and A. Javey, "Highly sensitive electronic whiskers based on patterned carbon nanotube and silver nanoparticle composite films," *Proc. Nat. Acad. Sci.*, vol. 111, no. 5, pp. 1703–1707, 2014.

[14] N. F. Lepora, M. Pearson, and L. Cramphorn, "Tacwhiskers: Biomimetic optical tactile whiskered robots," in *Proc. IEEE/RSJ Int. Conf. Intell. Robots Syst.*, 2018, pp. 7628–7634.

[15] B. Ward-Cherrier *et al.*, "The tactip family: Soft optical tactile sensors with 3D-printed biomimetic morphologies," *Soft Robot.*, vol. 5, no. 2, pp. 216–227, 2018.

[16] W. Yuan, S. Dong, and E. H. Adelson, "Gelsight: High-resolution robot tactile sensors for estimating geometry and force," *Sensors*, vol. 17, no. 12, 2017, Art. no. 2762.

[17] T. Feix, I. M. Bullock, and A. M. Dollar, "Analysis of human grasping behavior: Object characteristics and grasp type," *IEEE Trans. Haptics*, vol. 7, no. 3, pp. 311–323, May 2014.

[18] A. E.-T. Yang, M. J. Hartmann, and S. Bergbreiter, "Contact-resistive sensing of touch and airflow using a rat whisker," in *Proc. 7th IEEE Int. Conf. Biomed. Robot. Biomechatron.*, 2018, pp. 1187–1192.

[19] S. R. Anderson, M. J. Pearson, A. Pipe, T. Prescott, P. Dean, and J. Porrill, "Adaptive cancelation of self-generated sensory signals in a whisking robot," *IEEE Trans. Robot.*, vol. 26, no. 6, pp. 1065–1076, Dec. 2010.

[20] A. Yamaguchi and C. G. Atkeson, "Combining finger vision and optical tactile sensing: Reducing and handling errors while cutting vegetables," in *Proc. IEEE-RAS 16th Int. Conf. Humanoid Robots*, 2016, pp. 1045–1051.

[21] K. Vlack, T. Mizota, N. Kawakami, K. Kamiyama, H. Kajimoto, and S. Tachi, "Gelforce: A vision-based traction field computer interface," in *Proc. CHI'05 Extended Abstr. Hum. Factors Comput. Syst.*, 2005, pp. 1154–1155.

[22] D. S. Bolme, J. R. Beveridge, B. A. Draper, and Y. M. Lui, "Visual object tracking using adaptive correlation filters," in *Proc. IEEE Comput. Soc. Conf. Comput. Vis. Pattern Recognit.*, 2010, pp. 2544–2550.

[23] A. Lukezic, T. Vojir, L. Čehovin Zajc, J. Matas, and M. Kristan, "Discriminative correlation filter with channel and spatial reliability," in *Proc. IEEE Conf. Comput. Vis. Pattern Recognit.*, 2017, pp. 6309–6318.

[24] S. J. Prince, *Computer Vision: Models, Learning, and Inference*. Cambridge, U.K.: Cambridge Univ. Press, 2012.

[25] K. S. Severson, D. Xu, M. Van de Loo, L. Bai, D. D. Ginty, and D. H. Oâ-Connor, "Active touch and self-motion encoding by merkel cell-associated afferents," *Neuron*, vol. 94, no. 3, pp. 666–676.e9, May 2017.

[26] A. Wallach, K. Bagdasarian, and E. Ahissar, "On-going computation of whisking phase by mechanoreceptors," *Nat. Neurosci.*, vol. 19, no. 3, pp. 487–493, Mar. 2016.

[27] Y. S. W. Yu, M. M. Graff, and M. J. Z. Hartmann, "Mechanical responses of rat vibrissae to airflow," *J. Exp. Biol.*, vol. 219, no. 7, pp. 937–948, Apr. 2016.

[28] T. Kent, "Whisksight," 2020. [Online]. Avilable: https://github.com/TeresaAKent/WhiskSight